Dispersion Analysis of Displacement-Based and TDNNS Mixed Finite Elements for Thin-Walled Elastodynamics *

Dalibor Lukáš[†1] and Joachim Schöberl[2]

[1]VŠB–Technical University of Ostrava, 17. listopadu 15, 708 00 Ostrava-Poruba, Czech Republic.
[2]Vienna University of Technology, Wiedner Hauptstrasse 8-10, 1040 Wien, Austria.

Abstract

We compare several lowest-order finite element approximations to the problem of elastodynamics of thin-walled structures by means of dispersion analysis, which relates the parameter frequency-times-thickness (fd) and the wave speed. We restrict to analytical theory of harmonic front-crested waves that freely propagate in an infinite plate. Our study is formulated as a quasi-periodic eigenvalue problem on a single tensor-product element, which is eventually layered in the thickness direction. In the first part of the paper it is observed that the displacement-based finite elements align with the theory provided there are sufficiently many layers. In the second part we present novel anisotropic hexahedral tangential-displacement and normal-normal-stress continuous (TDNNS) mixed finite elements for Hellinger-Reissner formulation of elastodynamics. It turns out that one layer of such elements is sufficient for fd up to 2000 [kHz mm].

*This work was supported by the Czech Science Foundation under the project 17-22615S.

[†]Email: dalibor.lukas@vsb.cz

Nevertheless, due to a large amount of TDNNS degrees of freedom the computational complexity is only comparable to the multi-layer displacement-based element. This is not the case at low frequencies, where TDNNS is by far more efficient since it allows for rough anisotropic discretizations, contrary to the displacement-based elements that suffer from the shear locking effect.

Keywords: TDNNS mixed finite elements, elastodynamics, shear locking, dispersion analysis

1 Introduction

Finite element simulations of elastodynamics of thin-walled structures is an important means of nondestructive testing and structural health monitoring [Giu08, ZRK12]. Here the frequencies under consideration are typically ultrasonic and the simulation methods have to cover large spectrum of waves such as shear-horizontal or Lamb waves [Vik67]. The finite element method has to be robust with respect to both the thickness and frequency.

It is well-known that the standard displacement-based finite element methods suffer from the shear locking effect meaning that convergence of the finite element approximations deteoriates with decreasing aspect ratio of the geometry. Namely, the constant in Korn's inequality, which is an essential tool for the stability analysis, is proportional to this aspect ratio. For the mathematical theory on locking we refer to [BS92a, BS92b, SBS95]. There are basically two ways to overcome the shear locking.

Perhaps the most frequently used approach is to reduce the displacement-based elasticity to the theory of plates [BBH80, LMV98] and shells [CB03]. The plate theory can serve as the first level of a hirerachical modelling proposed by Babuška and Li [BL91], where one typically increases the order of the model in the thickness direction. For the analysis we also refer to [DFY04].

Another way of dealing with locking is to switch to the Hellinger-Reissner formulation of elasticity, where the displacement as well as stress field are computed simultaneously. The conforming method suggests the displacements to be left dicontinuous while the symmetric stress tensors preserve their normal component continuous. The first stable triangular element of this type was published as late as in 2002 by Arnold and Winther [AW02].

The lowest-order tetrahedral element was introduced by Adams and Cockburn [AC05] in 2005. It involves the following stress degrees of freedom (DOFs): 6 per vertex, 16 per edge, 9 per face, and 6 per element (bubbles). An extension to the arbitrary-order tetrahedron was published in 2008 by Arnold, Awanou, and Winther [AAW08]. The complexity can be avoided by imposing the symmetry of stress tensors only weakly by Lagrange multipliers. This leads to PEERS elements of plane elasticity [ABD84], which was proposed in 1984 by Arnold, Brezzi, and Douglas for problems with the Dirichlet boundary condition. It was generalized to arbitrary boundary conditions by Stenberg [Ste88]. In 2007 Arnold, Falk, and Winther [AFW07] proposed a 3-dimensional counterpart.

In this paper we follow yet another approach proposed in the Ph.D. thesis of Astrid Pechstein (born Sinwel) [Sin09] and published in a series of papers by Pechstein and Schöberl [PS11, PS12, PS17+]. The authors develop a new mixed method for the Hellinger-Reissner formulation of elasticity so that the displacements are searched in the $H(\mathrm{curl})$ Sobolev space, i.e., continuity of the tangential components of the displacements is preserved. It turns out that the stress tensors live in a new Sobolev space $H^{-1}(\mathrm{div}\,\mathrm{div})$, which can be approximated with symmetric stress tensors preserving continuity of the normal part of their normal components. The elements are referred to as tangential-displacement normal-normal-stresses (TDNNS). The lowest-order tetrahedral element [PS11] involves 2 displacement DOFs per edge, i.e., Nédélec-II [Ned86], 3 stress DOFs per face, and 12 stress bubbles (compare to those of [AC05]). In [PS12] a shear-locking free anisotropic prismatic element is proposed. In this paper we construct a hexahedral counterpart.

The aim of this paper is to show that the anisotropic TDNNS elements are robust not only regarding the thickness, but also the frequency. We shall numerically show that TDNNS covers analytical straight-crested wave theory of infinite plates [Giu08, Vik67]. It can be studied as a quasi-periodic quadratic eigenvalue problem [HFK06] on a single element or layered element. The rest of the paper is organized as follows: In Section 2 we recall analytical theory of straight-crested harmonic waves that freely propage in an infinite plate. In Section 3 the problem is reformulated as the quasi-periodic eigenvalue problem. We recall several 3d and 2d finite element approximations, each of which turns out to align well with the analytical theory. In Section 4 we recall the TDNNS method for the mixed formulation of elasticity. We construct a new stable hexahedral anisotropic element and show that only one layer can be sufficient to imitate the analytical theory in a large spectrum

of ultrasonic waves. In Section 5 we conclude with an observation that at low frequencies the novel TDNNS elements are superior since they allow for coarse discretizations into flat elements, hence, less degrees of freedom than corresponding fine discretizations into isotropic displacement-based elements.

2 Elastic guided waves in plates

We shall describe elastic waves that freely propagate in an infinite plate $\Omega := \mathbb{R}^2 \times (-d/2, d/2)$, where $d > 0$ is the thickness. We investigate the problem

$$\left\{ \begin{array}{rcl} \rho \frac{\partial^2}{\partial t^2} \mathbf{u}(x,t) - \mathbf{div}\, \boldsymbol{\sigma}(x,t) &=& \mathbf{0}, \quad x \in \Omega,\ t \in \mathbb{R}, \\ \boldsymbol{\sigma}(x,t) \cdot \mathbf{n}(x) &=& \mathbf{0}, \quad x \in \partial\Omega,\ t \in \mathbb{R}, \end{array} \right. \tag{1}$$

where $\rho > 0$, $\mathbf{u} : \Omega \times \mathbb{R} \to \mathbb{R}^3$, $\boldsymbol{\sigma} : \Omega \times \mathbb{R} \to \mathbb{R}^{3\times 3}_{\mathrm{sym}}$, and $\mathbf{n}$ are the density, the vectorial displacement field, the field of symmetric stress tensors, and the unit outward normal vector to Ω, respectively. The unknown displacements and stresses are related via the linear isotropic Hooke's law

$$\sigma_{ij} := \underbrace{\frac{E\,\nu}{(1+\nu)(1-2\,\nu)}}_{=:\lambda}\, \delta_{ij} \sum_{k=1}^{3} \varepsilon_{kk}(\mathbf{u}) + \underbrace{\frac{E}{1+\nu}}_{=:2\mu}\, \varepsilon_{ij}(\mathbf{u}), \tag{2}$$

where δ_{ij}, $E > 0$, $\nu \in (0, 1/2)$, and $\varepsilon_{kl}(\mathbf{u}) := \frac{1}{2}\left(\frac{\partial}{\partial x_l} u_k + \frac{\partial}{\partial x_k} u_l\right)$ denote the Kronecker delta, Young modulus, Poisson ratio, and strain tensor, respectively. The wave equation after eliminating the stress reads as follows:

$$\rho \frac{\partial^2}{\partial t^2} \mathbf{u}(x,t) - (\lambda + \mu)\, \nabla \operatorname{div}(\mathbf{u}(x,t)) - \mu \triangle \mathbf{u}(x,t) = \mathbf{0}. \tag{3}$$

Note that all the operators ∇, div, and $\triangle$ are applied with respect to the spatial variable x.

We shall restrict ourselves to harmonic waves propagating in the x_1-direction that are additionaly straight-crested, thus, x_2-invariant,

$$\mathbf{u}(x,t) = \mathrm{Re}\left\{ \begin{pmatrix} \widehat{u}_1(x_3) \\ \widehat{u}_2(x_3) \\ \widehat{u}_3(x_3) \end{pmatrix} \mathrm{e}^{i\kappa(x_1 - ct)} \right\}, \tag{4}$$

where $\omega := 2\pi f$ is the angular frequency, c is the wave speed, and $\kappa := \omega/c$ is the wave number. By inserting (4) into (3) and the boundary conditions in (1) we arrive at two separated problems. The first problem describing propagation of shear-horizontal waves reads as follows:

$$\begin{cases} \widehat{u}_2''(x_3) + (\kappa_{\mathrm{S}}^2 - \kappa^2)\,\widehat{u}_2(x_3) &= 0, \quad x_3 \in (-\frac{d}{2}, \frac{d}{2}), \\ \widehat{u}_2'\left(\frac{d}{2}\right) = \widehat{u}_2'\left(-\frac{d}{2}\right) &= 0, \end{cases}$$

where $\kappa_{\mathrm{S}} := \omega/c_{\mathrm{S}}$ and $c_{\mathrm{S}} := \sqrt{\mu/\rho}$. The differential equation admits solutions

$$\widehat{u}_2(x_3) = \widehat{A}\,\mathrm{e}^{i\sqrt{\kappa_{\mathrm{S}}^2-\kappa^2}x_3} + \widehat{B}\,\mathrm{e}^{-i\sqrt{\kappa_{\mathrm{S}}^2-\kappa^2}x_3}, \quad \widehat{A}, \widehat{B} \in \mathbb{C}.$$

The boundary conditions give the dispersion property, i.e., the velocities c at which the wave can propagate,

$$\frac{c}{c_{\mathrm{S}}} = \left[1 - \left(\frac{nc_{\mathrm{S}}}{2fd}\right)^2\right]^{-1/2},$$

where n is a nonnegative integer. Note that the waves related to n odd are referred to as antisymmetric, while n being zero or even is asociated with the symmetric shear-horizontal waves. Note also that the velocity depends on the parameter frequency-times-thickness, rather than the frequency alone. We depict the dispersion properties of the shear-horizontal waves in Fig. 1.

The other problem that arises after inserting (4) into (3) and (1) describes Lamb waves. It reads as follows:

$$\begin{cases} \widehat{u}_1''(x_3) + i\kappa(\gamma+1)\widehat{u}_3'(x_3) + (\gamma+2)\,(\kappa_{\mathrm{P}}^2 - \kappa^2)\,\widehat{u}_1(x_3) &= 0, \quad x_3 \in (-\frac{d}{2}, \frac{d}{2}), \\ (\gamma+2)\widehat{u}_3''(x_3) + i\kappa(\gamma+1)\widehat{u}_1'(x_3) + (\kappa_{\mathrm{S}}^2 - \kappa^2)\,\widehat{u}_3(x_3) &= 0, \quad x_3 \in (-\frac{d}{2}, \frac{d}{2}), \\ \widehat{u}_1'\left(\frac{d}{2}\right) + i\kappa\widehat{u}_3\left(\frac{d}{2}\right) &= 0, \\ \widehat{u}_1'\left(-\frac{d}{2}\right) + i\kappa\widehat{u}_3\left(-\frac{d}{2}\right) &= 0, \\ i\kappa\gamma\widehat{u}_1\left(\frac{d}{2}\right) + (\gamma+2)\widehat{u}_3'\left(\frac{d}{2}\right) &= 0, \\ i\kappa\gamma\widehat{u}_1\left(-\frac{d}{2}\right) + (\gamma+2)\widehat{u}_3'\left(-\frac{d}{2}\right) &= 0, \end{cases}$$

where we introduce $\gamma := \lambda/\mu$ and we denote by $c_{\mathrm{P}} := \sqrt{(\lambda+2\mu)/\rho}$ and $\kappa_{\mathrm{P}} := \omega/c_{\mathrm{P}}$ the speed of pressure waves and the related wave number. Note that $(\gamma+2)\kappa_{\mathrm{P}}^2 = \kappa_{\mathrm{S}}^2$. The differential equations admit solutions

$$\begin{aligned} \begin{pmatrix} \widehat{u}_1(x_3) \\ \widehat{u}_3(x_3) \end{pmatrix} = \widehat{C} \begin{pmatrix} \sqrt{\kappa_{\mathrm{S}}^2 - \kappa^2} \\ -\kappa \end{pmatrix} \mathrm{e}^{i\sqrt{\kappa_{\mathrm{S}}^2-\kappa^2}x_3} + \widehat{D} \begin{pmatrix} \sqrt{\kappa_{\mathrm{S}}^2 - \kappa^2} \\ \kappa \end{pmatrix} \mathrm{e}^{-i\sqrt{\kappa_{\mathrm{S}}^2-\kappa^2}x_3} \\ + \widehat{E} \begin{pmatrix} \kappa \\ \sqrt{\kappa_{\mathrm{P}}^2 - \kappa^2} \end{pmatrix} \mathrm{e}^{i\sqrt{\kappa_{\mathrm{P}}^2-\kappa^2}x_3} + \widehat{F} \begin{pmatrix} -\kappa \\ \sqrt{\kappa_{\mathrm{P}}^2 - \kappa^2} \end{pmatrix} \mathrm{e}^{-i\sqrt{\kappa_{\mathrm{P}}^2-\kappa^2}x_3}. \end{aligned}$$

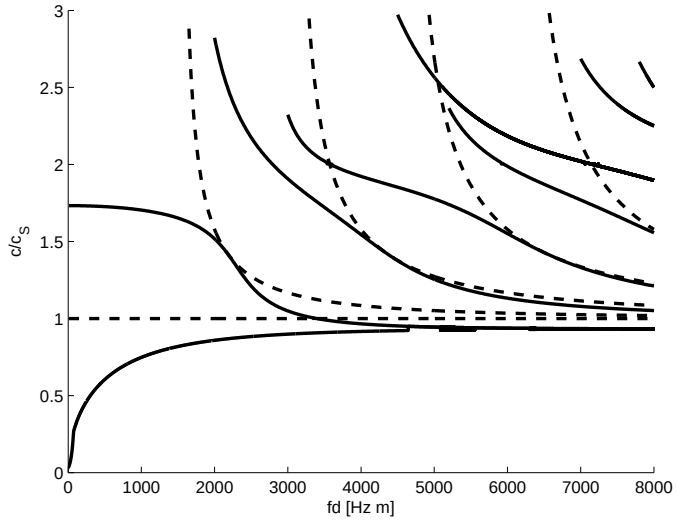

Figure 1: Dispersion properties of shear-horizontal waves (dashed lines) and Lamb waves (solid lines) propagating in an aluminium plate: $E := 69\,[\mathrm{GPa}]$, $\nu := 0.334$, $\rho := 2700\,[\mathrm{kg\,m^{-3}}]$.

The boundary conditions again specify the admissible velocities c. The dispersion relation is described by the equation

$$\det \begin{pmatrix} (\alpha^2-\kappa^2)\begin{pmatrix} \mathrm{e}^{i\alpha d/2} & -\mathrm{e}^{-i\alpha d/2} \\ \mathrm{e}^{-i\alpha d/2} & -\mathrm{e}^{i\alpha d/2} \end{pmatrix} & 2\kappa\beta \begin{pmatrix} \mathrm{e}^{i\beta d/2} & \mathrm{e}^{-i\beta d/2} \\ \mathrm{e}^{-i\beta d/2} & \mathrm{e}^{i\beta d/2} \end{pmatrix} \\ -2\kappa\alpha \begin{pmatrix} \mathrm{e}^{i\alpha d/2} & \mathrm{e}^{-i\alpha d/2} \\ \mathrm{e}^{-i\alpha d/2} & \mathrm{e}^{i\alpha d/2} \end{pmatrix} & (\alpha^2-\kappa^2)\begin{pmatrix} \mathrm{e}^{i\beta d/2} & -\mathrm{e}^{-i\beta d/2} \\ \mathrm{e}^{-i\beta d/2} & -\mathrm{e}^{i\beta d/2} \end{pmatrix} \end{pmatrix} = 0,$$

where $\alpha := \sqrt{\kappa_{\mathrm{S}}^2 - \kappa^2}$, $\beta := \sqrt{\kappa_{\mathrm{P}}^2 - \kappa^2}$. Note again that the velocity depends on the parameter frequency-times-thickness. The dispersion properties of the Lamb waves are depicted in Fig. 1.

3 Displacement-based FEM

We shall study the dispersion properties of the waves propagating in an infinite plate by means of various elastic finite element methods. In order to compare the FEM with the analytical theory we approximate the straight-

crested waves (4) as follows: First of all, to cover solutions harmonic in the x_1-direction we prescribe the quasi-periodic boundary conditions, see [HFK06],

$$\underbrace{\mathrm{e}^{i\kappa h}}_{=:\xi}\,\widehat{\mathbf{u}}(x) = \widehat{\mathbf{u}}(x_1+h,x_2,x_3), \quad \xi\widehat{\sigma}_{11}(x) = \widehat{\sigma}_{11}(x_1+h,x_2,x_3),$$

where $\widehat{\boldsymbol{\sigma}}$ is the harmonic counterpart of $\boldsymbol{\sigma}$. Therefore, the unbounded plate domain can be replaced by a bounded domain $\Omega^h := (0,h)^2 \times (-d/2,d/2)$, which is typically only one finite element. We denote by $\Gamma^h_{\mathrm{Q}} := \{0\} \times (0,h) \times (-d/2,d/2)$ the left part of the quasi-periodic boundary. Secondly, the x_2-invariance is replaced with the x_2-periodic boundary conditions and the choice of low-order finite element approximation in the x_2 direction. We denote by $\Gamma^h_{\mathrm{P}} := (0,h) \times \{0\} \times (-d/2,d/2)$ the front part of the periodic boundary. We complete the problem with the stress-free, i.e., Neumann boundary conditions on the bottom and top of Ω^h, $\Gamma^h_{\mathrm{N}} := (0,h)^2 \times \{-\frac{d}{2},\frac{d}{2}\}$. The problem now reads as follows: Find $\xi \in \mathbb{C}$, $|\xi| = 1$, and $\widehat{\mathbf{u}} : \Omega^h \to \mathbb{C}^3$ such that

$$\left\{\begin{array}{rcll} -\omega^2\rho\,\widehat{\mathbf{u}}(x) - (\lambda+\mu)\,\nabla\,\mathrm{div}\,\widehat{\mathbf{u}}(x) - \mu\,\triangle\,\widehat{\mathbf{u}}(x) &=& \mathbf{0}, & x \in \Omega^h, \\ \xi\widehat{\mathbf{u}}(x) - \widehat{\mathbf{u}}(x_1+h,x_2,x_3) &=& \mathbf{0}, & x \in \Gamma^h_{\mathrm{Q}}, \\ \xi\widehat{\boldsymbol{\sigma}}(x)\cdot\mathbf{n}(x) + \widehat{\boldsymbol{\sigma}}(x_1+h,x_2,x_3)\cdot\mathbf{n}(x_1+h,x_2,x_3) &=& \mathbf{0}, & x \in \Gamma^h_{\mathrm{Q}}, \\ \widehat{\mathbf{u}}(x) - \widehat{\mathbf{u}}(x_1,x_2+h,x_3) &=& \mathbf{0}, & x \in \Gamma^h_{\mathrm{P}}, \\ \widehat{\boldsymbol{\sigma}}(x)\cdot\mathbf{n}(x) &=& \mathbf{0}, & x \in \Gamma^h_{\mathrm{N}}. \end{array}\right. \tag{5}$$

The weak solution to (5) lives in the space of complex-valued functions

$$\widehat{\mathbf{V}}_\xi := \left\{\widehat{\mathbf{u}} \in [H^1(\Omega^h)]^3 : \widehat{\mathbf{u}} \text{ is } x_2\text{-periodic and } \xi\widehat{\mathbf{u}}(0,x_2,x_3) = \widehat{\mathbf{u}}(h,x_2,x_3)\right\}.$$

To get rid of the boundary term, we test (5) with functions from $\widehat{\mathbf{V}}_{\xi^*}$, where ξ^* is the complex conjugate. The weak formulation of (5) reads to find $\xi \in \mathbb{C}$, $|\xi| = 1$, and $\widehat{\mathbf{u}} \in \widehat{\mathbf{V}}_\xi$:

$$-\omega^2 \underbrace{\rho \int_{\Omega^h} \widehat{\mathbf{u}}\cdot\widehat{\mathbf{v}}}_{=:m(\widehat{\mathbf{u}},\widehat{\mathbf{v}})} + \underbrace{\int_{\Omega^h} (\mathbf{C}\cdot\boldsymbol{\varepsilon}(\widehat{\mathbf{u}}))\cdot\boldsymbol{\varepsilon}(\widehat{\mathbf{v}})}_{=:k(\widehat{\mathbf{u}},\widehat{\mathbf{v}})} = 0 \quad \forall\widehat{\mathbf{v}} \in \widehat{\mathbf{V}}_{\xi^*}, \tag{6}$$

where the Hooke's law (2) is now expressed in the Voigt notation,

$$\begin{pmatrix} \widehat{\sigma}_{11} \\ \widehat{\sigma}_{22} \\ \widehat{\sigma}_{33} \\ 2\widehat{\sigma}_{12} \\ 2\widehat{\sigma}_{13} \\ 2\widehat{\sigma}_{23} \end{pmatrix} = \underbrace{\begin{pmatrix} \lambda+2\mu & \lambda & \lambda & 0 & 0 & 0 \\ \lambda & \lambda+2\mu & \lambda & 0 & 0 & 0 \\ \lambda & \lambda & \lambda+2\mu & 0 & 0 & 0 \\ 0 & 0 & 0 & 4\mu & 0 & 0 \\ 0 & 0 & 0 & 0 & 4\mu & 0 \\ 0 & 0 & 0 & 0 & 0 & 4\mu \end{pmatrix}}_{=:\mathbf{C}} \cdot \underbrace{\begin{pmatrix} \varepsilon_{11}(\widehat{\mathbf{u}}) \\ \varepsilon_{22}(\widehat{\mathbf{u}}) \\ \varepsilon_{33}(\widehat{\mathbf{u}}) \\ \varepsilon_{12}(\widehat{\mathbf{u}}) \\ \varepsilon_{13}(\widehat{\mathbf{u}}) \\ \varepsilon_{23}(\widehat{\mathbf{u}}) \end{pmatrix}}_{=:\boldsymbol{\varepsilon}(\widehat{\mathbf{u}})}. \tag{7}$$

The FEM for the variational formulation (6), eventually its simplifications, see Sections 3.2 and 3.3, relies on basis functions $\widehat{\boldsymbol{\varphi}}_1(x)$, $\widehat{\boldsymbol{\varphi}}_2(x)$, $\ldots$,$\widehat{\boldsymbol{\varphi}}_n(x)$, the span of which approximates $[H^1(\Omega^h)]^3$. The x_2-periodicity is realized by a parameterization, i.e., a matrix $\mathbf{P} \in \mathbb{R}^{n\times p}$, where $p < n$ is the number of parameters. Finally, to implement the x_1-quasi-periodicity we divide the parameters into three distinct sets: the left parameters associated with $x_1 = 0$, the right parameters associated with $x_1 = h$, and the remaining inner parameters. We denoted these sets by L, R, and I, respectively. Without loss of generality we assume that $L = (1, 2, \ldots, |L|)$, $R = |L| + (1, 2, \ldots, |R|)$, where $|R| = |L|$, and $I = (2|L| + 1, \ldots, p)$. The FEM functions approximating $\widehat{\mathbf{V}}_\xi$ can be represented as follows:

$$\widehat{\mathbf{u}}(x) = \sum_{j=1}^{n} (\boldsymbol{\alpha})_j \widehat{\boldsymbol{\varphi}}_j(x), \quad \boldsymbol{\alpha} = \mathbf{P} \cdot \begin{pmatrix} \mathbf{p}_L \\ \xi\mathbf{p}_L \\ \xi\mathbf{p}_I \end{pmatrix},$$

while the FEM test functions approximating $\widehat{\mathbf{V}}_{\xi^*}$ admit the representation

$$\widehat{\mathbf{v}}(x) = \sum_{j=1}^{n} (\boldsymbol{\beta})_j \widehat{\boldsymbol{\varphi}}_j(x), \quad \boldsymbol{\beta} = \mathbf{P} \cdot \begin{pmatrix} \xi\mathbf{q}_R \\ \mathbf{q}_R \\ \xi\mathbf{q}_I \end{pmatrix}.$$

Thus, the FEM approximation to (6) reads to find $\xi \in \mathbb{C}$, $|\xi| = 1$, $\mathbf{p}_L \in \mathbb{C}^{|L|}$, and $\mathbf{p}_I \in \mathbb{C}^{|I|}$ such that $(\mathbf{p}_L, \mathbf{p}_I) \neq \mathbf{0}$ and

$$\begin{pmatrix} \xi\mathbf{q}_R \\ \mathbf{q}_R \\ \xi\mathbf{q}_I \end{pmatrix}^T \cdot \underbrace{\mathbf{P}^T \cdot (-\omega^2\mathbf{M} + \mathbf{K}) \cdot \mathbf{P}}_{=:\mathbf{A}_\omega} \cdot \begin{pmatrix} \mathbf{p}_L \\ \xi\mathbf{p}_L \\ \xi\mathbf{p}_I \end{pmatrix} = 0 \quad \forall \mathbf{q}_R \in \mathbb{C}^{|R|}, \mathbf{q}_I \in \mathbb{C}^{|I|},$$

where $(\mathbf{M})_{ij} := m(\widehat{\boldsymbol{\varphi}}_i(x), \widehat{\boldsymbol{\varphi}}_j(x))$ and $(\mathbf{K})_{ij} := k(\widehat{\boldsymbol{\varphi}}_i(x), \widehat{\boldsymbol{\varphi}}_j(x))$. After the substitution $\mathbf{r} := \xi\mathbf{p}$ we arrive at the generalized eigenvalue problem: Find $\xi \in \mathbb{C}$, $|\xi| = 1$, $\mathbf{p}_L \in \mathbb{C}^{|L|}$, $\mathbf{p}_I \in \mathbb{C}^{|I|}$ such that $(\mathbf{p}_L, \mathbf{p}_I) \neq \mathbf{0}$ and

$$\begin{pmatrix} -(\mathbf{A}_\omega)_{LL} - (\mathbf{A}_\omega)_{RR} & -(\mathbf{A}_\omega)_{RI} & -(\mathbf{A}_\omega)_{RL} & \mathbf{0} \\ -(\mathbf{A}_\omega)_{IL} & \mathbf{0} & \mathbf{0} & \mathbf{0} \\ \mathbf{I} & \mathbf{0} & \mathbf{0} & \mathbf{0} \\ \mathbf{0} & \mathbf{I} & \mathbf{0} & \mathbf{0} \end{pmatrix} \cdot \begin{pmatrix} \mathbf{r}_L \\ \mathbf{r}_I \\ \mathbf{p}_L \\ \mathbf{p}_I \end{pmatrix} = \xi \begin{pmatrix} (\mathbf{A}_\omega)_{LR} & (\mathbf{A}_\omega)_{LI} & \mathbf{0} & \mathbf{0} \\ (\mathbf{A}_\omega)_{IR} & (\mathbf{A}_\omega)_{II} & \mathbf{0} & \mathbf{0} \\ \mathbf{0} & \mathbf{0} & \mathbf{I} & \mathbf{0} \\ \mathbf{0} & \mathbf{0} & \mathbf{0} & \mathbf{I} \end{pmatrix} \cdot \begin{pmatrix} \mathbf{r}_L \\ \mathbf{r}_I \\ \mathbf{p}_L \\ \mathbf{p}_I \end{pmatrix}, \quad (8)$$

where $\mathbf{0}$ and $\mathbf{I}$ denote the zero and identity matrices of proper size.

The FEM counterpart of the dispersion diagram, i.e., the relation between c and fd is achieved via solutions to (8) in a range of $\omega := 2\pi f$, eventually, a range of d, so that the velocity c is calculated from the eigenvalues $\xi \in \mathbb{C}$, $|\xi| = 1$, by definition,

$$c = \frac{\omega\, h}{|\arg \xi|}.$$

Given an $h > 0$ the simulation is valid only for such range of $\omega \in (0, \omega_{\max}(h))$ within which the phase shift is reasonably small, e.g., $|\arg \xi| \in (0, \pi/2)$. To get valid results for larger ω we have to decrease h appropriately.

3.1 Hexahedral element

A natural idea is to build a conforming FEM approximation to (6). We start with the lowest-order hexahedral finite element, which comprises vectorial bilinear functions with the degrees of freedom at nodes, see Fig. 2 (left). The projection onto x_2-periodic functions is realized via the parameterization matrix

$$\mathbf{P} := \begin{pmatrix} \mathbf{P}_1 & \mathbf{0} & \mathbf{0} \\ \mathbf{0} & \mathbf{P}_1 & \mathbf{0} \\ \mathbf{0} & \mathbf{0} & \mathbf{P}_1 \end{pmatrix}, \text{ where } \mathbf{P}_1 := \begin{pmatrix} \mathbf{P}_0 & \mathbf{0} \\ \mathbf{0} & \mathbf{P}_0 \end{pmatrix} \text{ and } \mathbf{P}_0 := \begin{pmatrix} 1 & 0 \\ 0 & 1 \\ 0 & 1 \\ 1 & 0 \end{pmatrix}.$$

The left set comprises the odd indices $L := \{1, 3, 5, \ldots, 11\}$, while the right set comprises the even indices $R := \{2, 4, 6, \ldots, 12\}$ and $I := \emptyset$. The resulting FEM dispersion diagrams for the plate of the thickness $d := 1$ [mm]

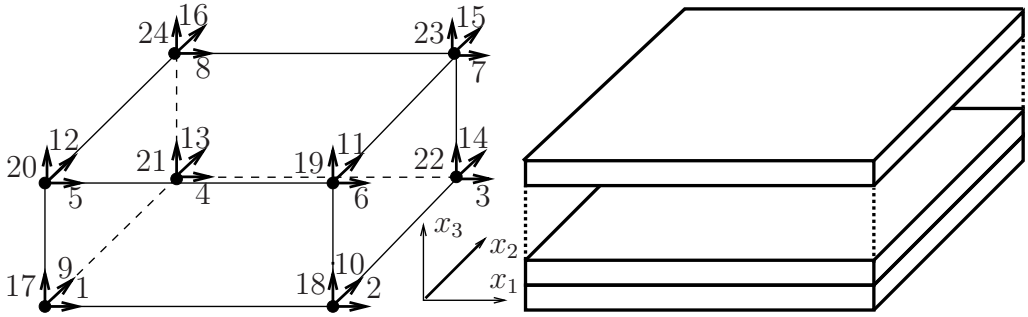

Figure 2: Displacement-based hexahedral element. (a) Degrees of freedom. (b) Multiple layers.

and two different discretization parameters $h := 1, 0.1$ [mm] are depicted in Fig. 3 (left). We can see that only two SH-modes, namely, the lowest order symmetric and antisymmetric ones are imitated properly in a large fd-range. Additionaly, these elements approximate the lowest-order symmetric and antisymmetric Lamb modes at small fd. This can be explained by the fact that the shapes of te eigenmodes in the thickness direction, $\mathrm{e}^{\pm i\alpha x_3}$ and $\mathrm{e}^{\pm i\beta x_3}$, are almost linear. To cope with the nonlinear shapes we introduce layers of the elements as depicted in Fig. 2 (right). The resulting FEM dispersion diagrams are depicted in Fig. 3 (right). We can see that while the discretization step $h := 1$ [mm] gives valid results only up to $fd = 200$ [Hz m], the step $h := 0.1$ [mm] yields correct dispersion behaviour roughly up to $fd = 4000$ [Hz m].

3.2 Plane-stress quadrilateral element

The simplest FEM imitating the shear waves assume the plane-stress ansatz, cf. [Bra01], $\sigma_{ij}(x,t) = \sigma_{ij}(x_1, x_2, t)$, $i, j = 1, 2$, and $\sigma_{3i}(x,t) = \sigma_{i3}(x,t) = 0$, $i = 1, 2, 3$, which implies $\varepsilon_{13} = \varepsilon_{23} = 0$ and $\varepsilon_{33} = -\frac{\lambda}{\lambda+2\mu}(\varepsilon_{11} + \varepsilon_{22})$. A compatible kinematics reads $u_i(x,t) = u_i(x_1, x_2, t)$, $i = 1, 2$, and $u_3(x,t) = x_3\, \varepsilon_{33}(x_1, x_2, t)$, but we have to neglect terms of order $O(x_3)$ in the strain

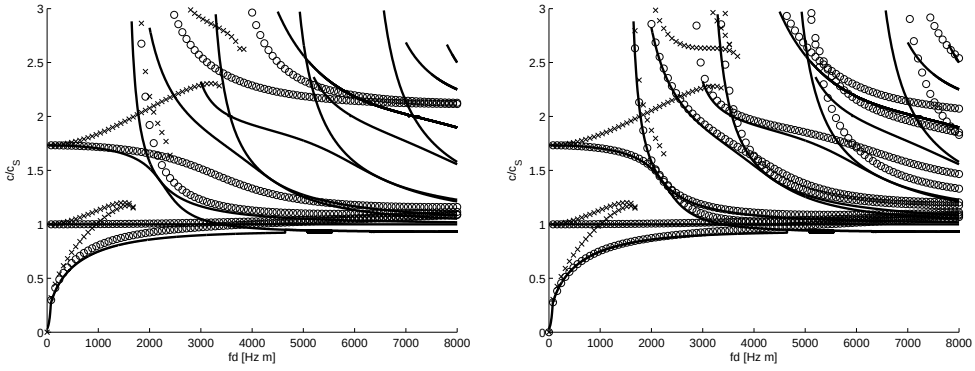

Figure 3: Displacement-based hexahedral finite element: Comparison of the analytical (solid line) and FEM dispersion diagrams for the aluminium plate, $d := 1\,[\mathrm{mm}]$. The FEM discretization parameter are $h := 1\,[\mathrm{mm}]$ (crosses) and $h := 0.1\,[\mathrm{mm}]$ (circles). (a) One layer. (b) Ten layers.

tensor. The bilinear forms in (6) changes,

$$\begin{aligned} m(\widehat{\mathbf{u}},\widehat{\mathbf{v}}) &= \rho\left\{ d\int_{(0,h)^2} \widehat{\mathbf{u}}\cdot\widehat{\mathbf{v}} + \frac{d^3}{12}\left(\frac{\lambda}{\lambda+2\mu}\right)^2 \int_{(0,h)^2} \mathrm{div}(\widehat{\mathbf{u}})\,\mathrm{div}(\widehat{\mathbf{v}})\right\}, \\ k(\widehat{\mathbf{u}},\widehat{\mathbf{v}}) &= d\int_{(0,h)^2} \left(\widetilde{\mathbf{C}}\cdot\widetilde{\boldsymbol{\varepsilon}}(\widehat{\mathbf{u}})\right)\cdot\widetilde{\boldsymbol{\varepsilon}}(\widehat{\mathbf{v}}), \end{aligned} \tag{9}$$

with the 2-dimensional complex-valued vectorial functions $\widehat{\mathbf{u}}$ and $\widehat{\mathbf{v}}$. The Hooke's law in the Voigt notation now reads as follows:

$$\begin{pmatrix} \widehat{\sigma}_{11} \\ \widehat{\sigma}_{22} \\ 2\widehat{\sigma}_{12} \end{pmatrix} = \underbrace{\begin{pmatrix} \widetilde{\lambda}+2\mu & \widetilde{\lambda} & 0 \\ \widetilde{\lambda} & \widetilde{\lambda}+2\mu & 0 \\ 0 & 0 & 4\mu \end{pmatrix}}_{=:\widetilde{\mathbf{C}}} \cdot \underbrace{\begin{pmatrix} \varepsilon_{11}(\widehat{\mathbf{u}}) \\ \varepsilon_{22}(\widehat{\mathbf{u}}) \\ \varepsilon_{12}(\widehat{\mathbf{u}}) \end{pmatrix}}_{=:\widetilde{\boldsymbol{\varepsilon}}(\widehat{\mathbf{u}})}, \tag{10}$$

where $\widetilde{\lambda} := \lambda\left(1-\frac{\lambda}{\lambda+2\mu}\right) = \frac{E\nu}{(1+\nu)(1-\nu)}$.

Assuming a small thickness, the second term in $m(\widehat{\mathbf{u}},\widehat{\mathbf{v}})$ can be neglected and we arrive at the 2-dimensional wave equation

$$-\omega^2\,\rho\,\widehat{\mathbf{u}} - (\widetilde{\lambda}+\mu)\,\nabla\mathrm{div}\,\widehat{\mathbf{u}} - \mu\,\triangle\,\widehat{\mathbf{u}} = \mathbf{0}.$$

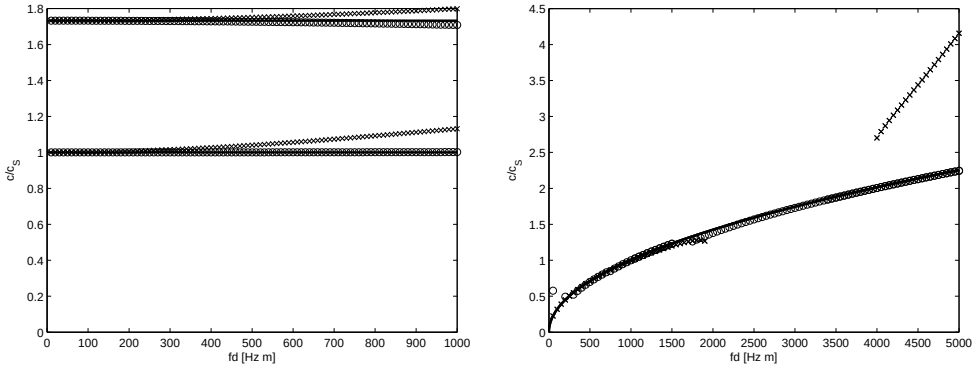

Figure 4: Displacement-based quadrilateral elements: Comparison of the analytical (solid line) and FEM dispersion diagrams for the aluminium plate, $d := 1\,[\mathrm{mm}]$. The FEM discretization parameter are $h := 1\,[\mathrm{mm}]$ (crosses) and $h := 0.1\,[\mathrm{mm}]$ (circles). (a) Quadrilateral plane-stress element. (b) Quadrilateral discrete Kirchohoff's plate element.

Restricting to the straight-crested ansatz (4) the waves become non-dispersive and they can propagate at two velocities,

$$\widetilde{c}_{\mathrm{S}} := c_{\mathrm{S}} := \sqrt{\frac{\mu}{\rho}} \text{ and } \widetilde{c}_{\mathrm{P}} := \sqrt{\frac{\widetilde{\lambda} + 2\mu}{\rho}}. \tag{11}$$

These correspond to the lowest-order symmetric shear-horizontal wave and the zero-frequency asymptotics of the lowest-order symmetric Lamb wave, see Fig. 1.

The lowest-order conforming quadrilateral finite element comprises vectorial bilinear functions with the degrees of freedom defined at nodes, similarly to the case of hexahedron. The resulting FEM dispersion diagrams for the plate of the thickness $d := 1$ [mm] and two different discretization parameters $h := 1, 0.1$ [mm] are depicted in Fig. 4 (left). The simulations align with the theory (11).

3.3 Discrete Kirchhoff's plate quadrilateral element

Similarly as in Section 3.2 we employ a dimensional reduction, but now we assume that the flat structure is loaded in the normal direction. The

ansatz, cf. [Bra01], reads as follows: $u_i(x,t) = -x_3 \frac{\partial}{\partial x_i} w(x_1,x_2,t)$, $i = 1,2$, $u_3(x,t) = w(x_1,x_2,t)$, and $\sigma_{33} = 0$, where the partial derivatives of the normal displacement w act as rotations. This again implies $\varepsilon_{13} = \varepsilon_{23} = 0$ and $\varepsilon_{33} = -\frac{\lambda}{\lambda+2\mu}(\varepsilon_{11} + \varepsilon_{22})$. Hence the 2d Hooke's law (10) holds. After neglecting the rotational inertia forces, (9) take the form

$$m(\widehat{w},\widehat{z}) = \rho\, d \int_{(0,h)^2} \widehat{w}\,\widehat{z}, \quad k(\widehat{w},\widehat{z}) = \frac{d^3}{12} \int_{(0,h)^2} \left(\widetilde{\mathbf{C}} \cdot \widetilde{\boldsymbol{\varepsilon}}(\nabla\widehat{w})\right) \cdot \widetilde{\boldsymbol{\varepsilon}}(\nabla\widehat{z}).$$

It is compatible with the 4-th order wave equation

$$-\omega^2\, \rho\, d\, \widehat{w} - \frac{d^3}{12} \operatorname{div}\left[(\widetilde{\lambda}+\mu)\, \nabla\operatorname{div}(\nabla\widehat{w}) + \mu\, \triangle(\nabla\widehat{w})\right] = 0.$$

Restricting to the straight-crested ansatz (4) the waves propagate at the velocity

$$c = \sqrt[4]{\frac{\widetilde{c}_{\mathrm{P}}}{12}}\sqrt{\omega\, d} \tag{12}$$

It corresponds to the zero-frequency asymptotics of the lowest-order anti-symmetric Lamb wave, see Fig. 1.

Besides continuity of the normal displacement $\widehat{w}$ a conforming FEM would also require continuity of $\nabla\widehat{w}$, hence a large amount of degrees of freedom. We employ the lowest-order discrete Kirchhoff's ansatz, cf. [BBH80, LMV98], where the continuity of gradients is required only at the nodes of the finite element, which is rectangle in our case. The element comprises of three degrees of freedom per node: one for the normal displacement and the others for its partial derivatives (rotations). The corresponding shape functions are reduced cubic polynomials for the displacements and reduced quadratic functions for the rotations. The resulting FEM dispersion diagrams for the plate of the thickness $d := 1$ [mm] and two different discretization parameters $h := 1, 0.1$ [mm] are depicted in Fig. 4 (right). The simulations align with the theory (12).

4 Mixed TDNNS formulation

In the mixed formulation we state not only the elastic motion equation (1), but also the Hooke's law (2) in the weak sense. Using the harmonic ansatz,

$$\mathbf{u}(x,t) = \operatorname{Re}\left\{\widehat{\mathbf{u}}(x)\, \mathrm{e}^{i\omega t}\right\}, \quad \boldsymbol{\sigma}(x,t) = \mathbf{Re}\left\{\widehat{\boldsymbol{\sigma}}(x)\, \mathrm{e}^{i\omega t}\right\},$$

the mixed formulation of (5) is to find $\xi \in \mathbb{C}$, $|\xi| = 1$, $\widehat{\mathbf{u}} \in \widehat{\mathbf{V}}_\xi$, and $\widehat{\boldsymbol{\sigma}} \in \widehat{\boldsymbol{\Sigma}}_\xi$ such that

$$\begin{array}{rcrcll} \int_{\Omega^h} (\mathbf{C}^{-1} \cdot \widehat{\boldsymbol{\sigma}}) \cdot \widehat{\boldsymbol{\tau}} & + & \langle \mathbf{div}\, \widehat{\boldsymbol{\tau}}, \widehat{\mathbf{u}} \rangle & = & 0 & \forall \widehat{\boldsymbol{\tau}} \in \widehat{\boldsymbol{\Sigma}}_{\xi^*}, \\ \langle \mathbf{div}\, \widehat{\boldsymbol{\sigma}}, \widehat{\mathbf{v}} \rangle & + & \omega^2 \rho \int_{\Omega^h} \widehat{\mathbf{u}} \cdot \widehat{\mathbf{v}} & = & 0 & \forall \widehat{\mathbf{v}} \in \widehat{\mathbf{V}}_{\xi^*}, \end{array} \tag{13}$$

where we employ the Voigt notation (7). Various choices of the spaces and the sesquilinear form $\langle ., . \rangle$ lead to different FEM methods. Letting $\widehat{\mathbf{V}}_\xi$ the meaning of Section 3, $\widehat{\boldsymbol{\Sigma}}_\xi := \left[L^2(\Omega^h)\right]^{3\times 3}_{\mathrm{sym}} \equiv \left[L^2(\Omega^h)\right]^6$ (Voigt notation), and $\langle \mathbf{div}\, \widehat{\boldsymbol{\sigma}}, \widehat{\mathbf{v}} \rangle := -\int_{\Omega^h} \widehat{\boldsymbol{\sigma}} \cdot \boldsymbol{\varepsilon}(\widehat{\mathbf{v}})$ leads to the displacement-based FEM of Section 3. On the other hand, $\widehat{\mathbf{V}}_\xi := \left[L^2(\Omega^h)\right]^3$, $\widehat{\boldsymbol{\Sigma}}_\xi \subset \left[\mathbf{H}(\mathrm{div}; \Omega^h)\right]^3_{\mathrm{sym}}$, and replacing the sesquilinear form by the L^2-inner product leads to the mixed FEM of [AW02, AC05]. The latter method suffers from the large amount of degrees of freedom to approximate the symmetric stress tensors.

Here we follow a compromise choice proposed by Astrid Pechstein (born Sinwel) in her Ph.D. thesis [Sin09], the results of which were also published in [PS11, PS12]. The displacements are searched in the Sobolev space

$$\widehat{\mathbf{V}}_\xi := \left\{ \widehat{\mathbf{u}} \in \mathbf{H}(\mathbf{curl}; \Omega^h) : \ \widehat{\mathbf{u}}_\mathbf{t} \text{ is } x_2\text{-per. and } \xi\, \widehat{\mathbf{u}}_\mathbf{t}(0, x_2, x_3) = \widehat{\mathbf{u}}_\mathbf{t}(h, x_2, x_3) \right\}$$

where the subscript $\mathbf{t}$ stands for the tangential component, which is the essential trace in $\mathbf{H}(\mathbf{curl}; \Omega^h)$. Further, let

$$\widehat{V}_\xi := \left\{ \widehat{u} \in H^1(\Omega^h) : \ \widehat{u} \text{ is } x_2\text{-per. and } \xi\, \widehat{u}(0, x_2, x_3) = \widehat{u}(h, x_2, x_3) \right\}.$$

The dual to the displacement spaces can be characterized as follows: $\widehat{\mathbf{V}}'_\xi = \left\{ \widehat{\mathbf{q}} \in \left[\widehat{V}'_\xi\right]^3 : \ \mathrm{div}\, \widehat{\mathbf{q}} \in \widehat{V}'_\xi \right\}$. Hence the sesquilinear form can be viewed as the duality pairing on $\widehat{\mathbf{V}}'_\xi \times \widehat{\mathbf{V}}_\xi$ and $\widehat{\mathbf{V}}'_{\xi^*} \times \widehat{\mathbf{V}}_{\xi^*}$. As a conclusion the stresses live in the following space:

$$\begin{aligned} \widehat{\boldsymbol{\Sigma}}_\xi := \Big\{ \widehat{\boldsymbol{\sigma}} \in \left[L^2(\Omega^h)\right]^{3\times 3}_{\mathrm{sym}} : \ & \mathrm{div}\, \mathbf{div}\, \widehat{\boldsymbol{\sigma}} \in \widehat{V}'_{\xi^*},\ \widehat{\sigma}_{\mathbf{nn}} \text{ is } x_2\text{-periodic}, \\ & \xi\, \widehat{\sigma}_{\mathbf{nn}}(0, x_2, x_3) = \widehat{\sigma}_{\mathbf{nn}}(h, x_2, x_3), \text{ and } \widehat{\sigma}_{\mathbf{nn}}(x) = 0 \text{ on } \Gamma^h_{\mathrm{N}} \Big\}, \end{aligned}$$

in which $\widehat{\sigma}_{\mathbf{nn}} := (\widehat{\boldsymbol{\sigma}} \cdot \mathbf{n}) \cdot \mathbf{n}$ is the essential trace. The essential traces, which are later used for the continuity of finite elements, give rise to the name tangential-displacement normal-normal-stress (TDNNS). For the fields that

are piecewise smooth over a finite element decomposition $\overline{\Omega^h} = \cup_K \overline{K}$ the sesquilinear form reads as follows:

$$\begin{aligned}\langle \mathbf{div}\, \widehat{\boldsymbol{\sigma}}, \widehat{\mathbf{v}} \rangle &= \sum_K \left(\int_K \mathbf{div}\, \widehat{\boldsymbol{\sigma}} \cdot \widehat{\mathbf{v}} - \int_{\partial K} \widehat{\boldsymbol{\sigma}}_{\mathbf{nt}} \cdot \widehat{\mathbf{v}}_{\mathbf{t}} \right) \\ &= \sum_K \left(- \int_K \widehat{\boldsymbol{\sigma}} \cdot \boldsymbol{\varepsilon}(\widehat{\mathbf{v}}) + \int_{\partial K} \widehat{\sigma}_{\mathbf{nn}}\, \widehat{v}_{\mathbf{n}} \right).\end{aligned}$$

4.1 Hexahedral anisotropic element

We introduce a novel anisotropic hexahedral TDNNS finite element. It follows construction of a prismatic element that was introduced and analyzed in [PS12].

Consider a tensor-product polygonal computational domain $\Omega := \Omega_{2d} \times (-d/2, d/2)$ and a finite element discretization $\mathcal{T}^h$ of Ω_{2d} into quadrilaterals, $\overline{\Omega_{2d}} = \cup_{Q \in \mathcal{T}^h} \overline{Q}$. Each hexahedron $K := Q \times (-d/2, d/2)$ is mapped from a reference cube $\widehat{K} := (0,1)^3$ using the trilinear shape functions $\lambda_{ijk}(\widehat{x}) := \lambda_i(\widehat{x}_1)\, \lambda_j(\widehat{x}_2)\, \lambda_k(\widehat{x}_3)$, $i,j,k = 1,2$, where $\lambda_1(t) := 1 - t$ and $\lambda_2(t) := t$, as follows:

$$K := \left\{ x = F^{(K)}(\widehat{x}) := \sum_{i,j,k=1}^{2} \lambda_{ijk}(\widehat{x})\, P_{ijk}^{(K)} : \ \widehat{x} \in \widehat{K} \right\},$$

where $P_{ijk}^{(K)}$ denote the vertices of K.

We appoximate the displacement space $\widehat{\mathbf{V}}_\xi$ in the conforming way using the lowest-order anisotropic Nédélec-II space

$$\widehat{\mathbf{V}}_\xi^h := \left\{ \widehat{\mathbf{v}}^h \in \widehat{\mathbf{V}}_\xi : \ \widehat{\mathbf{v}}^h|_K \circ F^{(K)} \in \left(\boldsymbol{\mathcal{P}}^1 \otimes \boldsymbol{\mathcal{P}}^2 \right) \times \left(\mathcal{P}^2 \otimes \mathcal{P}^1 \right) \ \forall K \right\},$$

where $\mathcal{P}^n$ denotes a scalar polynomial space over the interval $(0,1)$ and $\boldsymbol{\mathcal{P}}^n := (\mathcal{P}^n \otimes \mathcal{P}^n) \times (\mathcal{P}^n \otimes \mathcal{P}^n)$ denotes the 2d vectorial counterpart over $(0,1)^2$. Let $\mathbf{e}_d \in \mathbb{R}^3$ denote the d-th cartesian basis vector. We fulfil the $\mathbf{H}(\mathbf{curl}; \Omega)$-conformity, i.e., continuity of tangential components, by the following choice of displacement shape functions:

- 24 edge shapes: $m,n = 1,2$, $i = 0,1$,

$$\begin{aligned}\boldsymbol{\varphi}^{\mathrm{E}_1}_{1;m,n,i}(\widehat{x}) &:= q_i(\widehat{x}_1) \lambda_m(\widehat{x}_2) \lambda_n(\widehat{x}_3)\, \mathbf{e}_1, \\ \boldsymbol{\varphi}^{\mathrm{E}_2}_{2;m,n,i}(\widehat{x}) &:= q_i(\widehat{x}_2) \lambda_m(\widehat{x}_1) \lambda_n(\widehat{x}_3)\, \mathbf{e}_2, \\ \boldsymbol{\varphi}^{\mathrm{E}_3}_{3;m,n,i}(\widehat{x}) &:= q_i(\widehat{x}_3) \lambda_m(\widehat{x}_1) \lambda_n(\widehat{x}_2)\, \mathbf{e}_3,\end{aligned}$$

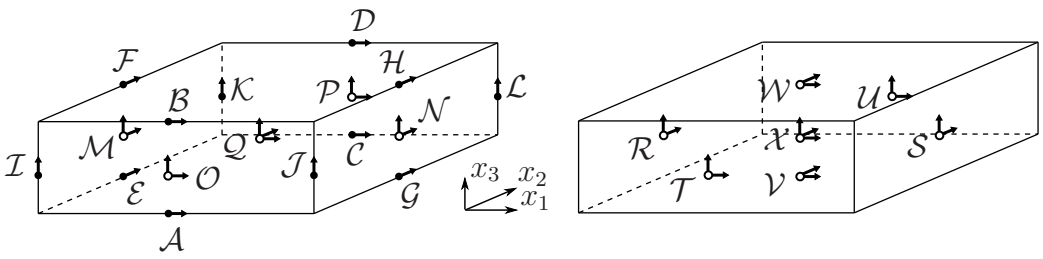

Figure 5: Mixed hexahedral TDNNS element: (a) Groups of displacement degrees of freedom — $\mathcal{A},\mathcal{B},\mathcal{C},\mathcal{D}$ comprise E_1-edge shapes; $\mathcal{E},\mathcal{F},\mathcal{G},\mathcal{H}$: E_2-edge shapes; $\mathcal{I},\mathcal{J},\mathcal{K},\mathcal{L}$: E_3-edge shapes; $\mathcal{M},\mathcal{N}$: F_1-face shapes; $\mathcal{O},\mathcal{P}$: F_2-face shapes; $\mathcal{Q}$: bubbles. (b) Groups of stress degrees of freedom — $\mathcal{R},\mathcal{S}$: F_1-vertical-face shapes; $\mathcal{T},\mathcal{U}$: F_2-vertical-face shapes; $\mathcal{V},\mathcal{W}$: F_3-horizontal-face shapes; $\mathcal{X}$: bubbles.

where $q_i(t)$ denote the Legendre polynomials: $q_0(t) := 1$, $q_1(t) := 2t-1$, $q_2(t) := \frac{1}{2}\,[3q_1(t)^2 - q_0(t)]$, etc.,

- 16 face shapes: $m = 1, 2$, $i = 0, 1$,

  $\boldsymbol{\varphi}^{\mathrm{F}_2}_{1;m,i}(\widehat{x}) := q_i(\widehat{x}_1)\lambda_m(\widehat{x}_2)\lambda_{12}(\widehat{x}_3)\,\mathbf{e}_1,\ \boldsymbol{\varphi}^{\mathrm{F}_1}_{2;m,i}(\widehat{x}) := q_i(\widehat{x}_2)\lambda_m(\widehat{x}_1)\lambda_{12}(\widehat{x}_2)\,\mathbf{e}_2,$
  $\boldsymbol{\varphi}^{\mathrm{F}_1}_{3;m,i}(\widehat{x}) := q_i(\widehat{x}_3)\lambda_m(\widehat{x}_1)\lambda_{12}(\widehat{x}_2)\,\mathbf{e}_3,\ \boldsymbol{\varphi}^{\mathrm{F}_2}_{3;m,i}(\widehat{x}) := q_i(\widehat{x}_3)\lambda_m(\widehat{x}_2)\lambda_{12}(\widehat{x}_1)\,\mathbf{e}_3,$

  where $\lambda_{12}(t) := \lambda_1(t)\lambda_2(t)$,

- and 2 element shapes (bubbles): $i = 0, 1$,

$$\boldsymbol{\varphi}^{\mathrm{B}}_{3;i}(\widehat{x}) := q_i(\widehat{x}_3)\lambda_{12}(\widehat{x}_1)\lambda_{12}(\widehat{x}_2)\,\mathbf{e}_3.$$

For a better understanding of the displacement shapes we also refer to Fig. 5 (left).

In order to get an inf-sup stable element the construction of the stress space follows the proof of the LBB-condition, see [Sin09, Lemma 4.17] or [PS11, Lemma 3.3]. First of all, on each face the normal-normal-stress components cover the space of normal-displacement jumps. They live in $\mathcal{P}^1 \otimes \mathcal{P}^1 \otimes \mathcal{P}^2$ on vertical faces and $\mathcal{P}^2 \otimes \mathcal{P}^2 \otimes \mathcal{P}^1$ on horizontal faces. This gives rise to the following stress shape functions:

- 24 vertical face shapes: $m = 1, 2$, $i = 0, 1$, $j = 0, 1, 2$,

  $\boldsymbol{\Psi}^{\mathrm{F}_1}_{1;m,i,j} := q_i(\widehat{x}_2)q_j(\widehat{x}_3)\lambda_m(\widehat{x}_1)\,\mathbf{E}_1,\ \boldsymbol{\Psi}^{\mathrm{F}_2}_{2;m,i,j} := q_i(\widehat{x}_1)q_j(\widehat{x}_3)\lambda_m(\widehat{x}_2)\,\mathbf{E}_2,$

- and 18 horizontal face shapes: $m = 1, 2,\ i, j = 0, 1, 2,$

$$\boldsymbol{\Psi}^{\mathrm{F}_3}_{3;m,i,j} := q_i(\widehat{x}_1) q_j(\widehat{x}_2) \lambda_m(\widehat{x}_3)\, \mathbf{E}_3,$$

where

$$\mathbf{E}_1 := \begin{pmatrix} 1 & 0 & 0 \\ 0 & 0 & 0 \\ 0 & 0 & 0 \end{pmatrix},\ \mathbf{E}_2 := \begin{pmatrix} 0 & 0 & 0 \\ 0 & 1 & 0 \\ 0 & 0 & 0 \end{pmatrix},\ \mathbf{E}_3 := \begin{pmatrix} 0 & 0 & 0 \\ 0 & 0 & 0 \\ 0 & 0 & 1 \end{pmatrix}.$$

Secondly, the element stress functions are based on the lowest-order normal-normal-free, i.e., bubble symmetric tensors. These are the following:

$$\mathbf{B}_d(\widehat{x}) := \lambda_{12}(\widehat{x}_d)\, \mathbf{E}_d,\ d = 1, 2, 3,$$
$$\mathbf{E}_{12} := \begin{pmatrix} 0 & 1 & 0 \\ 1 & 0 & 0 \\ 0 & 0 & 0 \end{pmatrix},\ \mathbf{E}_{13} := \begin{pmatrix} 0 & 0 & 1 \\ 0 & 0 & 0 \\ 1 & 0 & 0 \end{pmatrix},\ \mathbf{E}_{23} := \begin{pmatrix} 0 & 0 & 0 \\ 0 & 0 & 1 \\ 0 & 1 & 0 \end{pmatrix}.$$

To fulfil the discrete inf-sup condition the lowest-order stress bubbles has to be additionaly multiplied by tensor-product polynomials that live in the following image space of the strain operator of the local displacements:

$$\boldsymbol{\varepsilon}\left(\left(\boldsymbol{\mathcal{P}}^1 \otimes \boldsymbol{\mathcal{P}}^2\right) \times \left(\mathcal{P}^2 \otimes \mathcal{P}^1\right)\right) = \begin{pmatrix} \mathcal{P}^0 \otimes \mathcal{P}^1 \otimes \mathcal{P}^2 & \mathcal{P}^1 \otimes \mathcal{P}^1 \otimes \mathcal{P}^2 & \mathcal{P}^1 \otimes \mathcal{P}^2 \otimes \mathcal{P}^1 \\ \mathcal{P}^1 \otimes \mathcal{P}^1 \otimes \mathcal{P}^2 & \mathcal{P}^1 \otimes \mathcal{P}^0 \otimes \mathcal{P}^2 & \mathcal{P}^2 \otimes \mathcal{P}^1 \otimes \mathcal{P}^1 \\ \mathcal{P}^1 \otimes \mathcal{P}^2 \otimes \mathcal{P}^1 & \mathcal{P}^2 \otimes \mathcal{P}^1 \otimes \mathcal{P}^1 & \mathcal{P}^2 \otimes \mathcal{P}^2 \otimes \mathcal{P}^0 \end{pmatrix}.$$

This gives rise to the following stress shape functions:

- 21 diagonal bubbles: $i = 0, 1,\ j, k = 0, 1, 2,$

$$\boldsymbol{\Psi}^{\mathrm{B}}_{1;i,j}(\widehat{x}) := q_i(\widehat{x}_2) q_j(\widehat{x}_3)\, \mathbf{B}_1(\widehat{x}_1),\ \boldsymbol{\Psi}^{\mathrm{B}}_{2;i,j}(\widehat{x}) := q_i(\widehat{x}_1) q_j(\widehat{x}_3)\, \mathbf{B}_2(\widehat{x}_2),$$
$$\boldsymbol{\Psi}^{\mathrm{B}}_{3;k,j}(\widehat{x}) := q_k(\widehat{x}_1) q_j(\widehat{x}_2)\, \mathbf{B}_3(\widehat{x}_3),$$

- 36 off-diagonal bubbles: $i, j = 0, 1,\ k = 0, 1, 2,$

$$\boldsymbol{\Psi}^{\mathrm{B}}_{12;i,j,k}(\widehat{x}) := q_i(\widehat{x}_1) q_j(\widehat{x}_2) q_k(\widehat{x}_3)\, \mathbf{E}_{12},$$
$$\boldsymbol{\Psi}^{\mathrm{B}}_{13;i,j,k}(\widehat{x}) := q_i(\widehat{x}_1) q_j(\widehat{x}_3) q_k(\widehat{x}_2)\, \mathbf{E}_{13},$$
$$\boldsymbol{\Psi}^{\mathrm{B}}_{23;i,j,k}(\widehat{x}) := q_i(\widehat{x}_2) q_j(\widehat{x}_3) q_k(\widehat{x}_1)\, \mathbf{E}_{23}.$$

For a better understanding of the stress shapes we also refer to Fig. 5 (right).

Let $\boldsymbol{\Sigma}(\widehat{K})$ denote the (complex-valued) span of all the local stress shape functions. The (nonconforming) finite element approximation of $\widehat{\boldsymbol{\Sigma}}_\xi$ reads

$$\widehat{\boldsymbol{\Sigma}}^h_\xi := \Big\{ \widehat{\boldsymbol{\sigma}}^h \in \big[L^2(\Omega^h)\big]^{3\times 3}_{\mathrm{sym}} :\ \widehat{\sigma}^h_{\mathbf{nn}} \text{ is continuous },\ \widehat{\boldsymbol{\sigma}}^h|_K \circ F^{(K)} \in \boldsymbol{\Sigma}(\widehat{K})\ \forall K,$$
$$\widehat{\sigma}^h_{\mathbf{nn}} \text{ is } x_2\text{-per.},\ \xi\,\widehat{\sigma}^h_{\mathbf{nn}}(0,x_2,x_3) = \widehat{\sigma}^h_{\mathbf{nn}}(h,x_2,x_3),\ \text{and } \widehat{\sigma}^h_{\mathbf{nn}}(x) = 0 \text{ on } \Gamma^h_{\mathrm{N}} \Big\}.$$

Finally, to approximate solutions to (13) we shall define the projection matrix $\mathbf{P}$ realising the x_2-periodicity and the sets L, R, and I to impose the x_1-quasi-periodicity. Referring to Fig. 5, the projection matrix connects the following pairs of groups of degrees of freedom: $I_1 := \mathcal{A} \cup \mathcal{C}$, $I_2 := \mathcal{B} \cup \mathcal{D}$, $Q_1 := \mathcal{I} \cup \mathcal{J}$, $Q_2 := \mathcal{K} \cup \mathcal{L}$, $I_3 := \mathcal{O} \cup \mathcal{P}$, and $I_4 := \mathcal{T} \cup \mathcal{U}$. Moreover, to fulfil the stress-free boundary conditions we skip $\mathcal{V}$ and $\mathcal{W}$. The sets prescribing x_1-quasi-periodicity are as follows: $L := \mathcal{E} \cup \mathcal{F} \cup Q_1 \cup \mathcal{M} \cup \mathcal{R}$, $R := \mathcal{G} \cup \mathcal{H} \cup Q_2 \cup \mathcal{N} \cup \mathcal{S}$, and $I := I_1 \cup I_2 \cup I_3 \cup \mathcal{Q} \cup I_4 \cup \mathcal{X}$.

The resulting FEM dispersion diagrams for the plate of the thickness $d := 1$ [mm] and two different discretization parameters $h := 1, 0.1$ [mm] are depicted in Fig. 6 (left). We can see that the lowest order SH-modes as well as the lowest order Lamb modes are well approximated up to $fd = 4000$ [Hz m]. To cope with the higher order modes we employ layers, see Fig. 2 (right). In Fig. 6 (right) we can see that five layers are enough to imitate waves up to $fd = 8000$ [Hz m].

5 Conclusion

In this paper we compared several lowest-order elasticity finite elements by means of dispersion analysis for the analytical theory of harmonic front-crested waves that freely propagate in an infinite plate. It turned out that at ultrasonic frequencies several layers of the standard nodal displacement elements enjoy similarly good approximation properties as the novel TDNNS mixed finite elements.

We conclude with an observation that this is not the case at low frequencies, where we can make use of the fact that TDNNS does not suffer from the shear locking effect hence coarse discretizations into flat elements can be employed. Fig. 7 depicts that for fd up to 30 [Hz m] and a 1 [mm] thin plate it is sufficient to use $10 \times 10 \times 1$ [mm] elements. To get a comparable

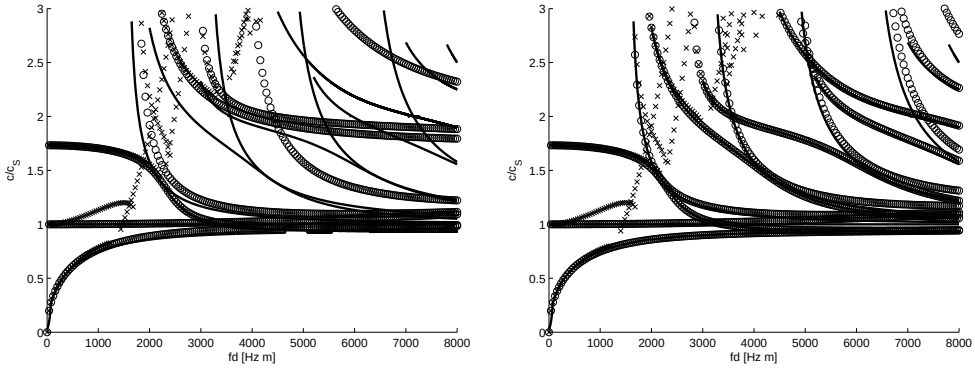

Figure 6: Mixed hexahedral TDNNS element: Comparison of the analytical (solid line) and FEM dispersion diagrams for the aluminium plate, $d := 1\,[\mathrm{mm}]$. The FEM discretization parameter are $h := 1\,[\mathrm{mm}]$ (crosses) and $h := 0.1\,[\mathrm{mm}]$ (circles). (a) One layer. (b) Five layers.

result with the displacement-based elements we need a thousand times more elements, namely, ten layers of $1 \times 1 \times 0.1\,[\mathrm{mm}]$ elements. Recall that after eliminating the bubbles there are 2 degrees of freedom per edge, 8 per vertical face, and 11 per horizontal face in case of TDNNS, while there are 3 degrees of freedom per node in case of the displacement-based FEM. Hence, comparable simulations in a $1 \times 1\,[\mathrm{m}]$ large plate with the thickness $1\,[\mathrm{mm}]$ would lead to systems with 10^5 and 10^7 degrees of freedom, respectively.

References

[AC05] Adams, S. and Cockburn, B.: A mixed finite element method for elasticity in three dimensions. Journal of Scientific Computing **25**(3), 515—521 (2005)

[ABD84] Arnold, D.N., Brezzi, F., and Douglas, J.: PEERS: A new mixed finite element for plane elasticity. Japan Journal of Industrial and Applied Mathematics **1**, 347—367 (1984)

[AW02] Arnold, D.N. and Winther, R.: Mixed finite elements for elasticity. Numerische Mathematik **92**(3), 401—419 (2002)

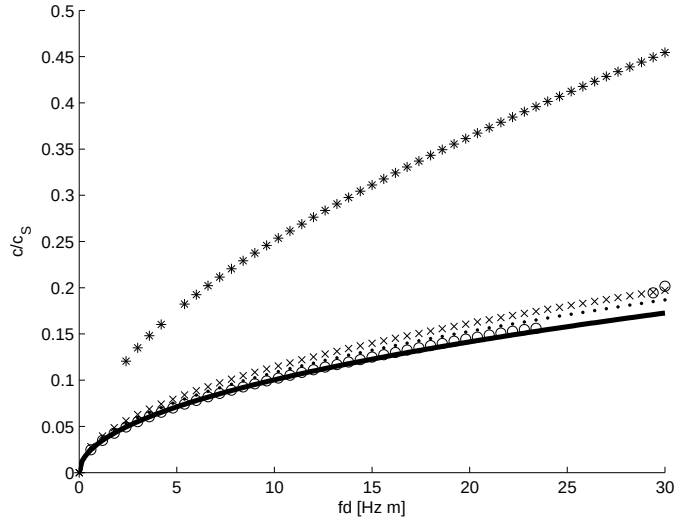

Figure 7: Comparison of the analytical solution (solid line), one-layer TDNNS FEM with $h := 10\,[\mathrm{mm}]$ (circles), one-layer displacement-based FEM with $h := 10\,[\mathrm{mm}]$ (stars), one-layer displacement-based FEM with $h := 1\,[\mathrm{mm}]$ (crosses), and 10-layers displacement-based FEM with $h := 1\,[\mathrm{mm}]$ (dots).

[AFW07] Arnold, D.N., Falk, R.S., and Winther, R.: Mixed finite element methods for linear elasticity with weakly imposed symmetry. Mathematics of Computation **76**(260), 1699—1723 (2007)

[AAW08] Arnold, D.N., Awanou, G., and Winther, R.: Finite elements for symmetric tensors in three dimensions. Mathematics of Computations **77**(263), 1229—1251 (2008)

[AL14] Arnold, D.N. and Lee, J.J.: Mixed methods for elastodynamics with weak symmetry. SIAM Journal on Numerical Analysis **52**(6), 2743—2769 (2014)

[BL91] Babuška, I. and Li, L.: Hierarchical modeling of plates. Computers and Structures **40**, 419—430 (1991)

[BS92a] Babuška, I. and Suri, M.: On locking and robustness in the finite element method. SIAM Journal on Numerical Analysis **29**(5), 1261—1293 (1992)

[BS92b] Babuška, I. and Suri, M.: Locking effects in the finite element approximation of elasticity problems. Numerische Mathematik **62**(1), 439—463 (1992)

[BBH80] Batoz, J.L., Bathe, K.J., and Ho, L.W.: A study of three-node triangular plate bending elements. International Journal for Numerical Methods in Engineering **15**(12), 1771—1812 (1980)

[BJT02] Bécache, E., Joly, P., and Tsogka, C.: A new family of mixed finite elements for the linear elastodynamic problem. SIAM Journal on Numerical Analysis **39**(6), 2109—2132 (2002)

[Bra01] Braess, D.: Finite Elements: Theory, Fast Solvers, and Applications in Elasticity Theory. Cambridge University Press (2001)

[CB03] Chapelle, D. and Bathe K.J.: The Finite Element Analysis of Shells — Fundamentals. Springer (2003)

[DFY04] Dauge, M., Faou, E., and Yosibash, Z.: Plates and shells: Asymptotic expansions and hierarchical models. In Stein, E., de Borst, R., and Hughes, T.J.R., Encyclopedia of Computational Mechanics, vol. 1, 199—236 (2004)

[Giu08] Giurgiutiu, V.: Structural Health Monitoring with Piezoelectric Wafer Active Sensors. Elsevier (2008)

[HFK06] Hofer, M., Finger, N., Kovacs, G., Schöberl, J., Zaglmayr, S., Langer, U., and Lerch, R.: Finite-element simulation of wave propagation in periodic piezoelectric SAW structures. IEEE Transactions on Ultrasonics, Ferroelectrics, and Frequency Control **53**(6), 1192—1201 (2006)

[Kri80] Křížek, M.: An equilibrium finite element method in three-dimensional elasticity. Applications of Mathematics **27**(1), 46—75 (1980)

[LMV98] LeTallec, P., Mandel, J., and Vidrascu, M.: A Neumann-Neumann domain decomposition algorithm for solving plate and shell problems. SIAM Journal on Numerical Analysis **35**(2), 836—867 (1998)

[Ned86] Nédélec, J.C.: A new family of mixed finite elements in $\mathbb{R}^3$. Numerische Mathematik **50**(1), 57—81 (1986)

[PS11] Pechstein, A. and Schöberl, J.: Tangential-displacement and normal-normal-stress continuous mixed finite elements for elasticity. Mathematical Models and Methods in Applied Sciences **21**(8), 1761—1782 (2011)

[PS12] Pechstein, A. and Schöberl, J.: Anisotropic mixed finite elements for elasticity. International Journal for Numerical Methods in Engineering **90**(2), 196—217 (2012)

[PS17+] Pechstein, A. and Schöberl, J.: An analysis of the TDNNS method using natural norms. Numerische Mathematik (submitted)

[Sin09] Sinwel, A.: A New Family of Mixed Finite Elements for Elasticity. Ph.D. thesis. Johannes Kepler University Linz (2009)

[Ste88] Stenberg, R.: A family of mixed finite elements for the elasticity problem. Numerische Mathematik **53**(5), 513—538 (1988)

[SBS95] Suri, M., Babuška, I., and Schwab, C.: Locking effects in the finite element approximation of plate models. Mathematics of Computation **64**(210), 461–482 (1995)

[Vik67] Viktorov, I.A.: Rayleigh and Lamb Waves: Physical Theory and Applications. Plenum Press, New York (1967)

[ZRK12] Zak, A., Radzieński, M., Krawczuk, M., and Ostachowicz, W.: Damage detection strategies based on propagation of guided elastic waves. Smart Materials and Structures **21**(3), 18 pp. (2012)